crystals

MDPI

Article

Heteroleptic [Cu(P^P)(N^N)][PF$_6$] Complexes: Effects of Isomer Switching from 2,2′-biquinoline to 1,1′-biisoquinoline

Nina Arnosti, Marco Meyer, Alessandro Prescimone, Edwin C. Constable and Catherine E. Housecroft *

Department of Chemistry, University of Basel, BPR 1096, Mattenstrasse 24a, CH-4058 Basel, Switzerland; nina.arnosti@unibas.ch (N.A.); marco.meyer@unibas.ch (M.M.); alessandro.prescimone@unibas.ch (A.P.); edwin.constable@unibas.ch (E.C.C.)

* Correspondence: catherine.housecroft@unibas.ch; Tel: +41-61-207-1008

Abstract: The preparation and characterization of [Cu(POP)(biq)][PF$_6$] and [Cu(xantphos)(biq)][PF$_6$] are reported (biq = 1,1'-biisoquinoline, POP = bis(2-(diphenylphosphanyl)phenyl)ether, and xantphos = (9,9-dimethyl-9*H*-xanthene-4,5-diyl)bis(diphenylphosphane). The single crystal structure of [Cu(POP)(biq)][PF$_6$] 0.5Et$_2$O was determined and compared to that in three salts of [Cu(POP)(bq)]$^+$ in which bq = 2,2'-biquinoline. The P–C–P angle is 114.456(19)^o in [Cu(POP)(biq)]$^+$ compared to a range of 118.29(3)–119.60(3)^o [Cu(POP)(bq)]$^+$. There is a change from an intra-POP PPh$_2$-phenyl/(C$_6$H$_4$)$_2$O-arene π-stacking in [Cu(POP)(biq)]$^+$ to a π-stacking contact between the POP and bq ligands in [Cu(POP)(bq)]$^+$. In solution and at ambient temperatures, the [Cu(POP)(biq)][PF$_6$]$^+$ and [Cu(xantphos)(biq)]$^+$ cations undergo several concurrent dynamic processes, as evidenced in their multinuclear NMR spectra. The photophysical and electrochemical behaviors of the heteroleptic copper (I) complexes were investigated, and the effects of changing from bq to biq are described. Short Cu···O distances within the [Cu(POP)(biq)]$^+$ and [Cu(xantphos)(biq)]$^+$ cations may contribute to their very low photoluminescent quantum yields.

Keywords: copper; bisphosphane; 1,1'-biisoquinoline; 2,2'-biquinoline; single crystal structure

Citation: Arnosti, N.; Meyer, M.; Prescimone, A.; Constable, E.C.; Housecroft, C.E. Heteroleptic [Cu(P^P)(N^N)][PF$_6$] Complexes: Effects of Isomer Switching from 2,2′-biquinoline to 1,1′-biisoquinoline. *Crystals* **2021**, *11*, 185. https://doi.org/10.3390/cryst11020185

Academic Editor: Ana Garcia-Deibe
Received: 27 January 2021
Accepted: 11 February 2021
Published: 13 February 2021

1. Introduction

Following the seminal studies of McMillin [1,2], heteroleptic copper (I) complexes [Cu(P^P)(N^N)]$^+$ in which N^N is a diimine and P^P is a bisphosphane are currently exploited for their emissive [3–8] and photocatalytic [9–11] properties. This family of complexes possesses low-lying metal-to-ligand charge transfer (MLCT) excited states, which often exhibit thermally activated delayed fluorescence (TADF) characteristics [8]. The P^P ligand is usually a wide bite-angle bisphosphane such as commercially available bis(2-(diphenylphosphanyl)phenyl)ether (POP) or (9,9-dimethyl-9*H*-xanthene-4,5-diyl)bis(diphenylphosphane) (xantphos). The chelating N^N ligand is most commonly a derivative of 2,2'-bipyridine (bpy) or 1,10-phenanthroline (phen) (Scheme 1). Upon photoexcitation, the copper (I) coordination sphere in [Cu(P^P)(N^N)]$^+$ undergoes flattening as Cu(I) is formally oxidized to Cu(II) in the MLCT state. This distortion exposes the metal center to attack by, for example, solvent molecules and is detrimental to the photophysical behavior since it can lead to emission quenching. Although POP and xantphos (Scheme 2) both offer steric protection within the coordination sphere of the copper center, additional shielding is gained by introducing substituents in the 6,6'-positions of bpy or 2,9-positions of phen. In earlier studies, we showed that 6-methyl, 6-ethyl, 6-phenyl, and 6-phenylthio substituents in the bpy ligand are particularly advantageous for the photophysical properties of [Cu(POP)(bpy)]$^+$ and [Cu(xantphos)(bpy)]$^+$ complexes [12–14].

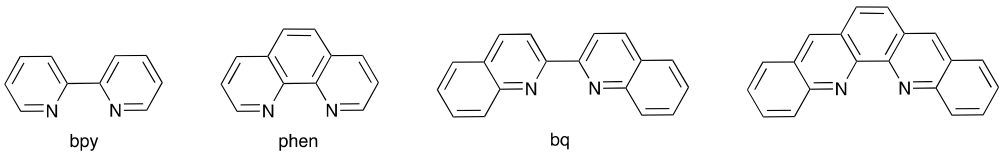

Scheme 1. Structures of 2,2'-biquinoline (bq) and dibenzo[b,j][1,10]phenanthroline compared to bpy and phen.

Another approach to increasing the steric demands of the N^N ligand is to replace bpy with 2,2'-biquinoline, or phen with dibenzo[b,j][1,10]phenanthroline (Scheme 1) [15–21]. Use of the bq ligand also has the advantage of extending the light absorption of the $[Cu(P^P)(N^N)]^+$ complex towards longer wavelengths. $[Cu(POP)(bq)]^+$ was first reported by Wang and coworkers, who reasoned that increasing the rigidity of the N^N ligand should lead to a decrease in non-radiative decay [15]. For 2,9-Me_2phen-containing (2,9-Me_2phen = 2,9-dimethyl-1,10-phenanthroline) heteroleptic copper (I) complexes, replacing two PPh_3 ligands with POP significantly enhances both the photoluminescence quantum yield (PLQY) and excited state lifetime (τ) [22,23]. However, the values of PLQY and τ were lower for $[Cu(POP)(bq)][BF_4]$ than for $[Cu(PPh_3)_2(bq)][BF_4]$ [15]. Interest in bq-containing $[Cu(P^P)(N^N)]^+$ complexes continued with the utilization of $[Cu(xantphos)(bq)][PF_6]$ and $[Cu(xantphos)(dmebq)][PF_6]$ (dmebq = dimethyl 2,2'-biquinoline-4,4'-dicarboxylate) as photosensitizers. Stabilization of the LUMO by introducing the electron withdrawing ester groups leads to a shift in the absorption maximum from 455 nm in $[Cu(xantphos)(bq)][PF_6]$ to 505 nm in $[Cu(xantphos)(dmebq)][PF_6]$ [17]. As with $[Cu(POP)(bq)][BF_4]$ [15], $[Cu(xantphos)(bq)][PF_6]$ and $[Cu(xantphos)(dmebq)][PF_6]$ are both weakly emitting, although White and coworkers confirmed that the bq unit provides sufficient steric protection to the copper center to minimize flattening of the coordination sphere in the excited state [17]. A comparison of the photophysical and photocatalytic properties of $[Cu(POP)(bq)]^+$ and $[Cu(xantphos)(bq)]^+$ demonstrated that the greater flexibility of the POP backbone imparts a lower photosensitizer stability with respect to ligand redistribution and formation of $[Cu(bq)_2]^+$ in solution [18]. In contrast to weak emission in solution for bq-containing complexes [15,17,18,21], Costa and coworkers reported that, in the solid-state or in thin films, $[Cu(POP)(deebq)][PF_6]$ and $[Cu(xantphos)(deebq)][PF_6]$ (deebq = diethyl 2,2'-biquinoline-4,4'-dicarboxylate) exhibit PLQY values in the range of 13–56%. $[Cu(POP)(deebq)][PF_6]$ and $[Cu(xantphos)(deebq)][PF_6]$ exhibit solid-state photoluminescence emission maxima at 676 and 671 nm, respectively, and were employed in light-emitting electrochemical cells (LECs) to yield deep-red emitting devices [20].

Growing interest in the use of derivatives of bq in $[Cu(P^P)(N^N)]^+$ complexes motivated us to investigate related complexes containing the isomeric 1,1'-biisoquinoline (biq, Scheme 2). Atropisomers are stereoisomers arising as a result of hindered rotation about a single bond, and atropisomerism is a form of axial chirality [24]. Atropisomerism is commonly observed when aromatic rings are connected by a single C–C bond, with the barrier to rotation arising from interactions between substituents on the aromatic rings. The descriptors *P* and *M* are used for right- or left-handed helicity about the C–C bond, respectively. 1,1'-Biisoquinolines have a chiral axis defined by the C1–C1' bond (Scheme 3). Attempts to resolve biq via the tartrate salt were unsuccessful, with mutarotation occurring within 80 seconds in 0.3 M hydrochloric acid solution [25]. Copper(I)-containing complexes of biq have been little explored, being limited to $[Cu(biq)_2][ClO_4]$ [26] and to Cu(I) derivatives of related ligands such as 1,12-diazaperylene [27] and its derivatives [28]. We report here the synthesis and characterization of $[Cu(POP)(biq)][PF_6]$ and $[Cu(xantphos)(biq)][PF_6]$ and assess the consequences of incorporating 1,1'-biisoquinoline rather than 2,2'-biquinoline on structural, electrochemical, and photophysical properties. Scheme 2 summarizes the ligands used in this work.

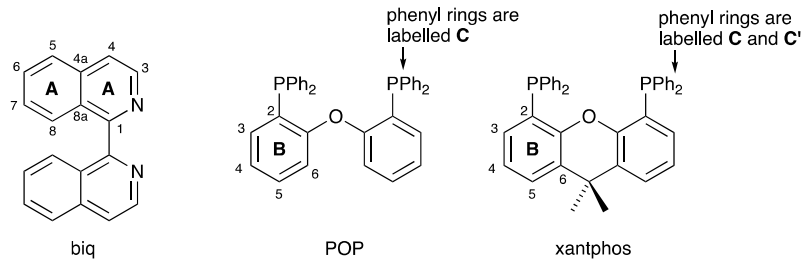

Scheme 2. Structures of 1,1'-biisoquinoline (biq), bis(2-(diphenylphosphanyl)phenyl)ether (POP), and (9,9-dimethyl-9*H*-xanthene-4,5-diyl)bis(diphenylphosphane) (xantphos) with atom labelling used for NMR spectroscopic assignments.

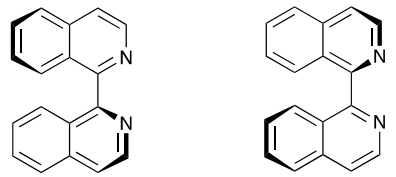

Scheme 3. Atropisomers of biq.

2. Materials and Methods

2.1. General

^{1}H, ^{13}C{^{1}H}, and ^{31}P{^{1}H} NMR spectra were recorded at 298 K on a Bruker Avance III-500 or Bruker Avance-III 600 NMR spectrometer (Bruker BioSpin AG, Fällanden, Switzerland). ^{1}H and ^{13}C NMR chemical shifts were referenced to residual solvent peaks with respect to δ(TMS) = 0 ppm and ^{31}P NMR chemical shifts with respect to δ(85% aqueous H_3PO_4) = 0 ppm. A Shimadzu LCMS-2020 instrument was used to record electrospray (ESI) mass spectra (Shimadzu Schweiz GmbH, 4153 Reinach, Switzerland). Solution absorption and solution emission spectra were measured using a Shimadzu UV2600 spectrometer and a Shimadzu RF-5301PC spectrofluorometer, respectively. A Hamamatsu absolute photoluminescence quantum yield spectrometer C11347 Quantaurus-QY (Hamamatsu Photonics France, 4500 Solothurn) was used to measure PLQYs, and powder emission spectra were measured using a Hamamatsu Compact Fluorescence lifetime Spectrometer C11367 Quantaurus-Tau with an LED light source (λ_{exc} = 365 nm) (Hamamatsu, 4500 Solothurn, Switzerland). Electrochemical measurements were conducted using a CH Instruments 900B potentiostat (CH Instruments, Austin, United States) and a VersaSTAT 3F (AMETEK Princeton Applied Research, Oak Ridge, United States) with [^{n}Bu$_4$N][PF$_6$] (0.1 M) as the supporting electrolyte and a scan rate of 0.1 V s^{-1}; the solvent used was CH_2Cl_2. The working electrode was glassy carbon, the reference electrode was a leakless Ag^{+}/AgCl electrode (eDAQ ET069-1), and the counter electrode was a platinum wire. Final potentials were internally referenced with respect to the Fc/Fc^{+} couple.

POP and xantphos were purchased from Acros (Fisher Scientific AG, Reinach, Switzerland) and Fluorochem (Chemie Brunschwig AG, Basel, Switzerland), respectively. 1,1'-The preparation of biisoquinoline was based on the procedure described for 3,3'-dimethyl-1,1'-biisoquinoline [28]. [Cu(MeCN)$_4$][PF$_6$] was synthesized as reported by Kubas et al [29]. [Cu(POP)(bq)][PF$_6$] and [Cu(xantphos)(bq)][PF$_6$] were prepared by standard procedures (the same methods as for the biq complexes in Sections 2.2 and 2.3) and their spectroscopic properties matched those reported in the literature [15,17].

2.2. [Cu(POP)(biq)][PF6]

[Cu(MeCN)4][PF6] (130 mg, 0.350 mmol) and POP (207 mg, 0.385 mmol) were dissolved in CH_2Cl_2 (30 mL) and stirred for 1 h at around 22 °C. Then, biq (89.7 mg, 0.350 mmol) was added and the reaction mixture was stirred for 1 h. After filtration, the solvent was removed from the filtrate under reduced pressure. The crude product was dissolved in the minimum amount of CH_2Cl_2. Then, Et_2O (3 × 10 mL) was added to precipitate the product. The solid was separated by centrifugation (9000 rpm, 4 min) and was dried under reduced pressure. [Cu(POP)(biq)][PF6] was isolated as an orange solid (331 mg, 0.330 mmol, 94.3%). ^{1}H-NMR (500 MHz, $(CD_3)_2CO$, 298 K) δ/ppm 8.59 (d, J = 5.8 Hz, 2H, H^{A3}), 8.12 (dd, J = 8.7, 1.2 Hz, 2H, H^{A5}), 7.96 (overlapping m, 4H, H^{A6+A8}), 7.82 (d, J = 5.7 Hz, 2H, H^{A4}), 7.71 (m, 2H, H^{A7}), 7.45 (m, 2H, H^{B5}), 7.31 (t, J = 7.5 Hz, 2H, $H^{C4/C4'}$), 7.25 (m, 2H, H^{B6}), 7.20 (t, J = 7.4 Hz, 2H, $H^{C4/C4'}$), 7.14–7.03 (overlapping m, 14H, $H^{B4+C3+C3'+C2/C2'}$), 6.98 (m, 4H, $H^{C2/C2'}$), 6.80 (m, 2H, H^{B3}). ^{13}C{^{1}H}-NMR (126 MHz, $(CD_3)_2CO$, 298 K) δ/ppm 159.5 (C^{B1}), 155.6 ($C^{A1/A4a/A8a}$), 143.0 (C^{A3}), 137.9 ($C^{A1/A4a/A8a}$), 135.3 (C^{B3}), 134.2 (t, J_{PC} = 8 Hz, $C^{C2/C2'}$), 133.6 (t, J_{PC} = 8 Hz, $C^{C2/C2'}$), 133.3 (C^{B5}), 132.7 ($C^{A6/A8}$), 132.0 (m, C^{C1}), 131.0 ($C^{C4/C4'}$), 130.8 ($C^{C4/C4'}$), 129.6 (C^{A7}), 129.5 (t, J_{PC} = 5 Hz, $C^{C3+C3'}$), 128.6 ($C^{A1/A4a/A8a}$), 128.5 ($C^{A6/A8}$), 128.45 (C^{A5}), 126.2 (C^{B4}), 124.9 (C^{A4}), 124.7 (C^{B2}), 121.5 (C^{B6}). ^{31}P{^{1}H}-NMR (202 MHz, $(CD_3)_2CO$, 298 K) δ/ppm −13.3 (POP), −144.2 (septet, J_{PF} = 707 Hz, $[PF_6]^-$). ESI MS: m/z 857.16 $[M-PF_6]^+$ (base peak, calc. 857.19), 601.04 $[Cu(POP)]^+$ (calc. 601.09). Found C 64.38, H, 4.00, N 2.94; $C_{54}H_{40}CuF_6N_2OP_3$ requires C 64.64, H 4.02, N 2.79.

2.3. [Cu(xantphos)(biq)][PF6]

The method was the same as that for [Cu(POP)(biq)][PF6] starting with [Cu(MeCN)4][PF6] (130 mg, 0.350 mmol, 1.0 eq.), xantphos (223 mg, 0.385 mmol, 1.1 eq.), and biq (89.7 mg, 0.350 mmol, 1.0 eq.) [Cu(xantphos)(biq)][PF6] was isolated as an orange solid (242 mg, 0.232 mmol, 66.3%). ^{1}H-NMR (600 MHz, $C_2D_2Cl_4$, 328 K) δ/ppm 7.95 (d, J = 8.3 Hz, 2H, H^{A8}), 7.93 (d, J = 5.8 Hz, 2H, H^{A3}), 7.88 (m, 2H, H^{A7}), 7.81 (d, J = 8.7 Hz, 2H, H^{A5}), 7.71 (dd, J = 7.8, 1.4 Hz, 2H, H^{B5}), 7.65 (m, 2H, H^{A6}), 7.62 (d, J = 5.8 Hz, 2H, H^{A4}), 7.25–7.20 (overlapping m, 4H, $H^{B4+C4/C4'}$), 7.09 (m, 2H, $H^{C4/C4'}$), 6.95 (t, J = 7.8 Hz, 4H, $H^{C3/C3'}$), 6.89–6.83 (overlapping m, 8H, $H^{C3/C3'+C2/C2'}$), 6.68 (m, 4H, $H^{C2/C2'}$), 6.54 (m, 2H, H^{C3}), 1.82 (s, 6H, $H^{xantphos-Me}$). ^{13}C{^{1}H}-NMR (150 MHz, $C_2D_2Cl_4$, 328 K) δ/ppm 154.5 (C^{B1}), 154.4 ($C^{A1/A4a/A8a}$), 141.5 (C^{A3}), 136.5 ($C^{A1/A4a/A8a}$), 133.7 (C^{B6}), 132.9 (t, J_{PC} = 8 Hz, $C^{C2/C2'}$), 131.8 (C^{A7} overlapping with t, J_{PC} = 8 Hz, $C^{C2/C2'}$), 131.1 (C^{B3}), 130.6 (t, J_{PC} = 16 Hz, $C^{C1/C1'}$), 130.3 (t, J_{PC} = 16 Hz, $C^{C1/C1'}$), 130.0 ($C^{C4/C4'}$), 129.6 ($C^{C4/C4'}$), 129.0 (C^{A6}), 128.5 (t, J_{PC} = 5 Hz, $C^{C3/C3'}$), 128.2 (t, J_{PC} = 5 Hz, $C^{C3/C3'}$), 127.5 (C^{A8+B5}), 127.2 ($C^{A1/A4a/A8a}$), 126.8 (C^{A5}), 125.1 (C^{B4}), 123.7 (C^{A4}), 119.5 (t, J_{PC} = 14 Hz, C^{B2}), 35.8 ($C^{xantphos-bridge}$), 28.3 ($C^{xantphos-Me}$). ^{31}P{^{1}H}-NMR (242 MHz, $C_2D_2Cl_4$, 328 K) δ/ppm −13.5 (xantphos), −144.3 (septet, J_{PF} = 714 Hz, $[PF_6]^-$). ESI MS: m/z 897.16 $[M-PF_6]^+$ (base peak, calc. 897.22), 641.07 $[Cu(xantphos)]^+$ (calc. 641.12). Found C 65.58, H, 4.73, N 2.40; $C_{57}H_{44}CuF_6N_2OP_3$ requires C 65.61, H 4.25, N 2.68.

2.4. Crystallography

Single crystal data were collected on a STOE StadiVari diffractometer equipped with a Pilatus300K detector and with a Metaljet D2 source (GaKα radiation) and by solving the structure using Superflip [30,31] and Olex2 [32]. The structure was refined using ShelXL v. 2014/7 [33]. The program CSD Mercury 2020.1 [34] was used for the structure analysis and structural figures. The Et_2O solvent molecule was disordered over a symmetry element and was modelled over two positions each with an occupancy of 0.5.

[Cu(POP)(biq)][PF6] 0.5Et_2O: $C_{56}H_{45}CuF_6N_2O_{1.5}P_3$, M_r = 1040.39, yellow block, triclinic, space group P–1, a = 11.4728(3), b = 14.2115(4), c = 16.0992(4) Å, α = 92.018(2), β = 91.054(2), γ = 112.546(2)°, V = 2421.34(12) Å^3, D_c = 1.427 g cm^{-3}, T = 150 K, Z = 2, μ(GaKα) = 3.409 mm^{-1}. Total 33,930 reflections, 10,023 unique (R_{int} = 0.0577). Refinement of 9750 reflections (625 parameters) with $I > 2\sigma(I)$ converged at final R_1 = 0.0457 (R_1 all data = 0.0468), wR_2 = 0.1252 (wR_2 all data = 0.1269), gof = 1.032. CCDC 2056169.

3. Results

3.1. Preparation and Characterization of [Cu(POP)(biq)][PF$_6$] and [Cu(xantphos)(biq)][PF$_6$]

The reactions of [Cu(NCMe)$_4$][PF$_6$], biq, and either POP or xantphos resulted in the formation of the orange compounds [Cu(POP)(biq)][PF$_6$] and [Cu(xantphos)(biq)][PF$_6$], respectively. After purification, the complexes were isolated in 94.3% and 66.3% yields, respectively. For each compound, the base peak in the ESI mass spectrum corresponded to the [M–PF$_6$]$^+$ ion (*m*/*z* = 857.16 for [Cu(POP)(biq)]$^+$ and *m*/*z* = 897.16 for [Cu(xantphos)(biq)]$^+$). The only other peak observed arose from the [Cu(P^P)]$^+$ ion (*m*/*z* = 601.04 for POP and *m*/*z* = 641.07 for xantphos) (Figures S1 and S2 in the Supplementary Materials).

X-ray quality single crystals of [Cu(POP)(biq)][PF$_6$] 0.5Et$_2$O were grown by diffusion of Et$_2$O into a CH$_2$Cl$_2$ solution of the complex. The compound crystallizes in the triclinic space group *P*–1, and Figure 1 depicts the structure of the [Cu(POP)(biq)]$^+$ cation present in the asymmetric unit. Two enantiomers are present in the unit cell with opposite senses of the axial chirality of the chiral axis (the C1–C1' bond of 1,1'-biisoquinoline) with one exhibiting (1*P*) and the other exhibiting (1*M*) chirality. The atom Cu1 is in a distorted tetrahedral environment, and the bond lengths and angles within the coordination sphere are given in the caption to Figure 1a. While the Cu1–N2 bond length of 2.0495(17) Å is typical, Cu1–N1 is noticeably lengthened (2.1434(16) Å), and this is possibly associated with a weak C–H···π interaction [35,36], involving the C1H1 unit and the arene ring containing C25 (C1H1···ring-plane = 2.78 Å and C1H1···centroid = 3.35 Å). The P–C bond lengths lie in the range 1.817(2) to 1.8315(19) Å. The Cu1···O1 separation is 3.054(1) Å, and this is towards the shorter end of the range of values observed for [Cu(POP)(N^N)]$^+$ complexes; we return to this point in Section 3.4 [37]. The torsion angle N1–C5–C6–N2 is –38.5(2)° and the angle between the least-squares planes of the rings containing N1 and N2 is 43.7°. The twist in the biq ligand leads to each Cu–N bond vector being non-coincidental with the direction of the lone pair of the *sp*^{2} hybridized N atom [38], as shown in Figure S3 in the Supplementary Materials. The angle subtended by the Cu–N vector and the plane of the corresponding NC$_5$ ring is 30.8° for N1 and 22.1° for N2. Figure 1b illustrates that the POP ligand adopts a conformation that leads to a π-stacking interaction between a phenyl ring of one PPh$_2$ group and an arene ring of the (C$_6$H$_4$)$_2$O unit. Within the π-stacking contact, the angle between the planes of the rings containing C31 and C38 is 20.8° and the inter-centroid distance is 3.80 Å. This π-stacking interaction is a common motif within the structurally characterized [Cu(POP)(N^N)]$^+$ cations found in the Cambridge Structural Database (CSD version 5.4.1 searched using Conquest version 2020.2.0 [39,40]). The phenyl ring containing C19 (Figure 1a) is oriented such that the C20–H20 unit is directed towards the CuN$_2$C$_2$-chelate ring with a CH···centroid distance of 2.56 Å. This adds to the steric protection around the copper center.

1,1'-Biisoquinoline (biq) is distinct from its isomer 2,2'-biquinoline (bq), not only in possessing axial chirality, as discussed in the Introduction, but also in its steric requirements within the coordination sphere of a metal to which it is bound. We were therefore interested in comparing the structures of the [Cu(POP)(biq)]$^+$ and [Cu(POP)(bq)]$^+$ cations. The single crystal structures of [Cu(POP)(bq)][PF$_6$] 0.5CH$_2$Cl$_2$ 0.2H$_2$O [19], [Cu(POP)(bq)][BF$_4$] 2MeOH [15], and [Cu(POP)(bq)][PF$_6$] CF$_3$SO$_3$ 0.6H$_2$O [41] have previously been reported, and important structural data are given in Table 1 and are compared with the corresponding data for [Cu(POP)(biq)][PF$_6$] 0.5Et$_2$O. The structures of the [Cu(POP)(bq)]$^+$ cations are compared in Figure 2. Cu–N and Cu–P bond lengths lie in typical ranges. While the P–Cu–P bond angle in [Cu(POP)(bq)]$^+$ is little affected by a change in the counterion (Table 1), it is noticeably larger in [Cu(POP)(bq)]$^+$ than in [Cu(POP)(biq)]$^+$ (114.456(19)°). The most significant change from [Cu(POP)(biq)]$^+$ (Figure 1) to [Cu(POP)(bq)]$^+$ (Figure 2) is the loss of the intramolecular PPh$_2$-phenyl/(C$_6$H$_4$)$_2$O-arene π-stacking interaction (Figure 2b). The torsion angles in Table 1 confirm that the bq ligand is closer to being planar than the sterically hindered biq. The N–C–C–N torsion

angles (defined in Figure 2) in the hexafluoridophosphate and triflate salts are similar (14.0 and 12.9°) but are larger than the 4.8° observed in the tetrafluoridoborate salt. Compare these torsion angles to the value of –38.5(2)° in [Cu(POP)(biq)][PF_6]. Although not discussed in the original report [15], Figure 3 illustrates that the near planarity of the 2,2'-biquinoline ligand is concomitant with face-to-face π-stacking with one phenyl ring of a PPh_2 unit of POP (centroid···centroid = 3.56 Å, angle between ring planes = 12.2°). This is reminiscent of the π-stacking interactions in [Cu(POP)(pyq)][PF_6], where pyq = 2-(pyridin-2-yl)quinoline [37]. Figure 2a,b illustrate the evolution of the π-stacking interaction in the [Cu(POP)(bq)]$^+$ cations in the hexafluoridophosphate and triflate salts, with the lack of an efficient interaction corresponding with the larger torsion angle of the bq ligand. The switch from PPh_2-phenyl/$(C_6H_4)_2O$-arene π-stacking in [Cu(POP)(biq)]$^+$ (i.e., an interaction within the POP domain) to an inter-ligand (but still intramolecular) π-stacking in [Cu(POP)(bq)]$^+$ is associated with the extended conjugation in the N^N ligand.

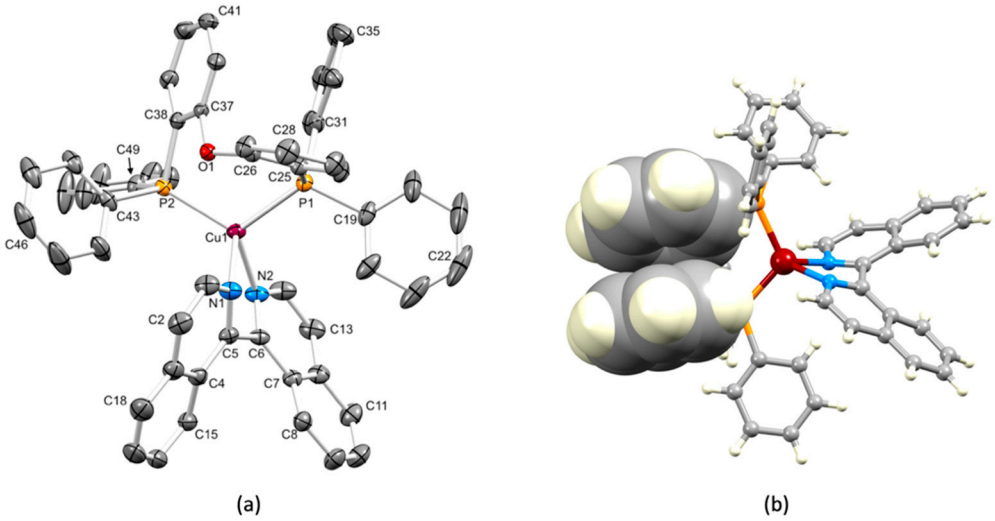

Figure 1. (**a**) An ORTEP-type plot of the [Cu(POP)(biq)]$^+$ cation in [Cu(POP)(biq)][PF_6]·0.5Et_2O with ellipsoids plotted at 40% probability level and H atoms omitted for clarity. Selected bond parameters: Cu1–P2 = 2.2480(5), Cu1–P1 = 2.2718(5), Cu1–N1 = 2.1434(16), Cu1–N2 = 2.0495(17), O1–C26 = 1.397(2), O1–C37 = 1.390(2), C6–C5 = 1.499(3) Å, P2–Cu1–P1 = 114.456(19), N1–Cu1–P2 = 114.32(5), N1–Cu1–P1 = 106.53(5), N2–Cu1–P2 = 123.53(5), N2–Cu1–P1 = 112.45(6), N2–Cu1–N1 = 79.30(6), C37–O1–C26 = 118.02(14)°. (**b**) Intramolecular π-stacking (space-filling representation) in the [Cu(POP)(biq)]$^+$ cation (see text).

Table 1. Comparison of crystal and selected structural parameters in salts of [Cu(POP)(bq)]$^+$ and [Cu(POP)(biq)][PF_6].

	[Cu(POP)(bq)][PF_6] 0.5CH_2Cl_2·0.2H_2O	**[Cu(POP)(bq)][CF_3SO_3] 0.6H_2O**	**[Cu(POP)(bq)][BF_4] 2MeOH**	**[Cu(POP)(biq)][PF_6] 0.5Et_2O**
Crystal system	Triclinic	Triclinic	Monoclinic	Triclinic
Space group	*P* – 1	*P* – 1	$P2_1/n$	*P*–1
Cu–N/Å	2.087(2), 2.075(2)	2.073(2), 2.093(2)	2.053(4), 2.067(5)	2.1434(16), 2.0495(17)
Cu–P/Å	2.2475(8), 2.2535(8)	2.2442(8), 2.2575(8)	2.2367(19), 2.3494(19)	2.2480(5), 2.2718(5)
Cu···O/Å	3.215(2)	3.241(2)	3.227(4)	3.054(1)
N–Cu–N/°	78.93(9)	79.2(1)	79.9(2)	79.30(6)
P–Cu–P/°	119.60(3)	118.29(3)	119.49 (7)	114.456(19)
Torsion [a] N–C–C–N/°	14.0	12.9	4.8	–38.5(2)
CSD refcode	CAPLIR	XIQTEZ	JITNIK	
Reference	[19]	[41]	[15]	This work

[a] The torsion angle is defined in Figure 2.

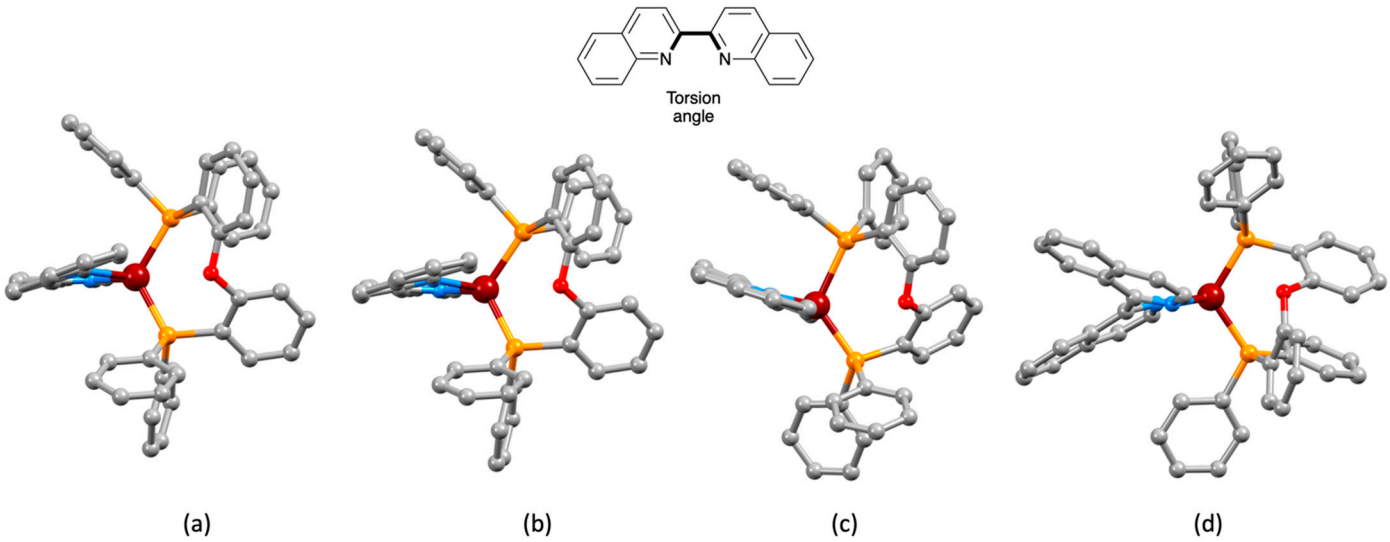

Figure 2. Crystallographically determined structures of the $[Cu(POP)(bq)]^+$ cation in (**a**) $[Cu(POP)(bq)][PF_6]$ $0.5H_2O$ $0.5CH_2Cl_2$, (**b**) $[Cu(POP)(bq)][PF_6]$ CF_3SO_3 $0.6H_2O$, and (**c**) $[Cu(POP)(bq)][BF_4]$ 2MeOH. The figures were generated using coordinates from the Cambridge Structural Database (CSD) refcodes CAPLIR, XIQTEZ, and JITNIK, respectively. (**d**) The structure of the $[Cu(POP)(biq)]^+$ cation (this work) for comparison. The N–C–C–N torsion angle in Table 1 is defined in the diagram at the top.

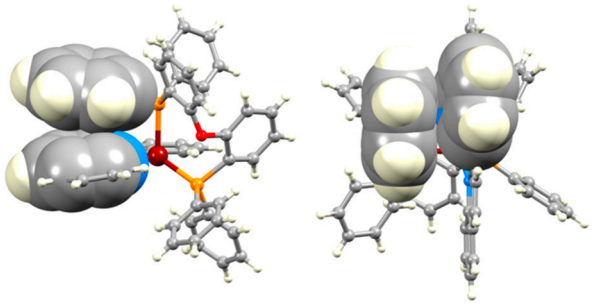

Figure 3. Two views of the face-to-face π-stacking in the $[Cu(POP)(bq)]^+$ cation in $[Cu(POP)(bq)][BF_4]$ 2MeOH (CSD refcode JITNIK [15]).

X-ray-quality single crystals of $[Cu(xantphos)(biq)][PF_6]$ could not be obtained, and therefore, we calculated the energy minimized structure of the $[Cu(xantphos)(biq)]^+$ cation to gain insight into the relationship between the N^N and P^P ligands within the copper coordination sphere. The structure was first minimized at a molecular mechanics (MM2) level, and this geometry was used as the input for a density functional theory (DFT) level energy minimization (B3LYP 6-31G*) [42]. The calculated structure of $[Cu(xantphos)(biq)]^+$ is shown in Figure 4, and Cartesian coordinates are presented in Table S1. Within the distorted tetrahedral environment of the copper atom, the P–Cu–P bond angle is 116.0°. The P–Cu–N bond angles of 111.9, 112.5, 114.8, and 117.2° lead to the biq ligand being skewed slightly towards the xanthene bowl (on the left of Figure 4a). This is related to the hosting of the C3–H3 unit of the biq ligand within the bowl-like cavity of the xanthene unit (Figure 4b). This is relevant to the NMR spectroscopic discussion to follow. A short Cu···O distance of 3.08 Å is found in the calculated structure, and this is similar to the crystallographically determined Cu···O distance of 3.054(1) Å in $[Cu(xantphos)(biq)][PF_6]$.

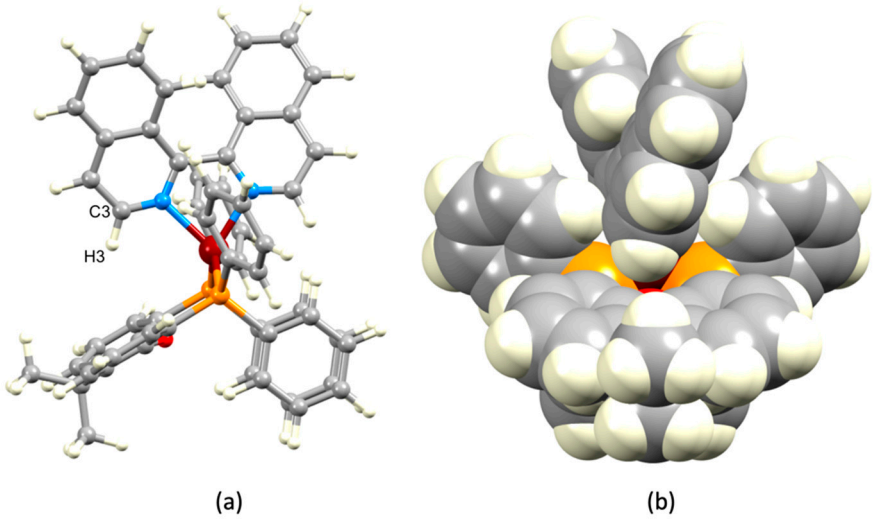

Figure 4. Calculated structure of the $[Cu(xantphos)(biq)]^+$ cation showing (**a**) a distorted tetrahedral Cu(I) coordination sphere and (**b**) accommodation of the C3–H3 unit of the biq ligand within the bowl-like cavity of the xanthene unit.

3.2. NMR Spectroscopy

The solution NMR spectra of [Cu(POP)(biq)][PF_6] and [Cu(xantphos)(biq)][PF_6] were recorded in acetone-d_6 solutions at 298 K, but for [Cu(xantphos)(biq)][PF_6], the signals were broad (Figure S3a in the Supplementary Materials). In order to carry out NMR spectroscopic measurements at higher temperatures, the solvent was changed to $C_2D_2Cl_4$. Even at 298 K, this led to sharp signals (Figure S3b), presumably due to the differences in viscosities and dielectric constants of the solvents. Warming the sample to 328 K did not lead to any significant changes in the ^{1}H NMR spectrum. Figure 5 shows the ^{1}H NMR spectra of [Cu(POP)(biq)][PF_6] in acetone-d_6 and [Cu(xantphos)(biq)][PF_6] in $C_2D_2Cl_4$ at 298 K. The ^{1}H and ^{13}C{^{1}H} NMR spectra were assigned using COSY, NOESY, HMQC, and HMBC spectra (the latter are displayed in Figures S6–S8). In [Cu(POP)(biq)][PF_6], proton H^{A3} (see Scheme 2 for atom numbering) is deshielded as a consequence of this proton being located over an arene ring of the POP backbone. (This corresponds to the weak C–H···π interaction described in the structural discussion above.) The corresponding signal in the xantphos-containing cation occurs at lower frequency (Figure 5), consistent with proton H^{A3} residing over the bowl-like cavity of the xanthene unit (Figure 4). This partly accounts for the large change in the resonance for H^{A3} from δ 8.59 ppm in [Cu(POP)(biq)][PF_6] to δ 7.93 ppm in [Cu(xantphos)(biq)][PF_6] (Figure 1). However, we note that the change in solvent from acetone-d_6 to $C_2D_2Cl_4$ also causes a shift to lower frequency for the signal for H^{A3} from δ 8.13 ppm to δ 7.93 ppm (Figure S3).

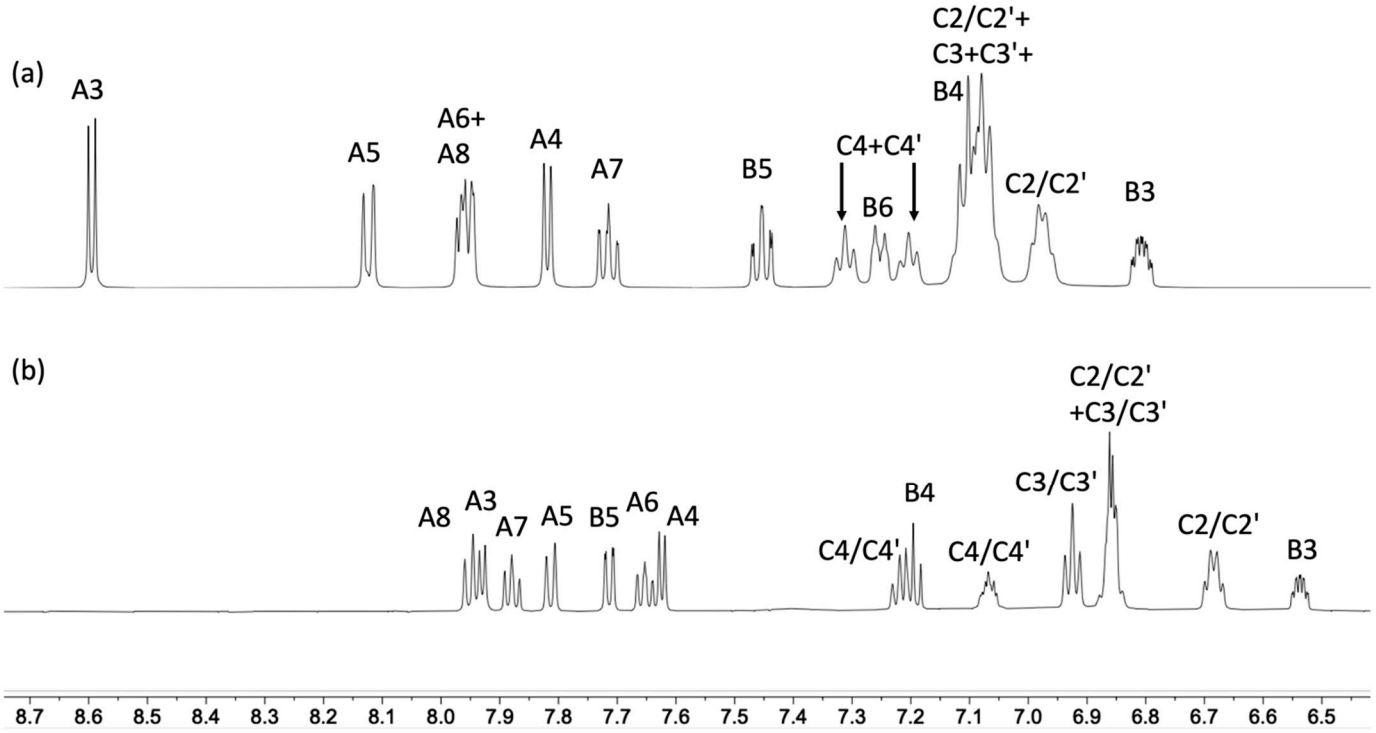

Figure 5. ^{1}H NMR spectra (aromatic region) of (a) [Cu(POP)(biq)][PF_6] (acetone-d_6, 500 MHz, 298 K) and (b) [Cu(xantphos)(biq)][PF_6] ($C_2D_2Cl_4$, 600 MHz, 298 K). See Scheme 2 for the atom labelling scheme.

The NMR spectra of the complexes are consistent with significant dynamic behavior in solution at ambient temperatures. We previously discussed the solution dynamics of related bpy-containing [Cu(POP)(N^N)]$^+$ and [Cu(xantphos)(N^N)]$^+$ complexes in detail; see, for example, [14,43]. In [Cu(POP)(biq)]$^+$ and [Cu(xantphos)(biq)]$^+$, several dynamic processes may be considered: (i) rotation about the P–C_{phenyl} bonds which is fast on the NMR timescale at 298 K; (ii) atropisomerization of the biq ligand (Scheme 4a); and (iii) a conformational change of the POP (Scheme 4b) or xantphos backbone (Scheme 4c). Atropisomerization of the coordinated biq ligand is expected to occur rapidly on the NMR timescale at 298 K [38,44]. Although Figure 4; Figure 5 show that the two isoquinoline units of the biq ligand are in different environments in the solid-state, the conformational changes in the POP or xantphos ligand shown in Scheme 4b,c render them equivalent on the NMR timescale. Figure 1 illustrates two phenyl environments (rings C and C'), corresponding to rings facing towards or away from the biq ligand. Exchange (EXSY) peaks are observed in the NOESY spectra of both [Cu(POP)(biq)][PF_6] and [Cu(xantphos)(biq)][PF_6] between $H^{C2/C2'}$, $H^{C3/C3'}$, and $H^{C4/C4'}$ (Figure 6). This is evidence for exchange between the pairs of phenyl rings in chemically different environments. However, the dynamic process is slow enough on the NMR timescale for separate resonances for phenyl rings C and C' to be observed.

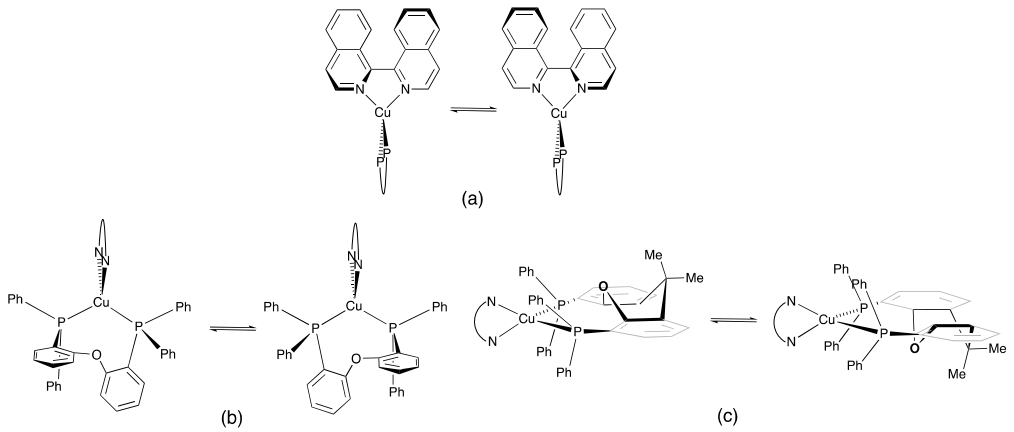

Scheme 4. Dynamic processes in [Cu(POP)(biq)]$^+$ and [Cu(xantphos)(biq)]$^+$: (a) atropisomerization of the coordinated biq, (b) conformational change of the POP backbone, and (c) conformational change of the xanthene unit in xantphos.

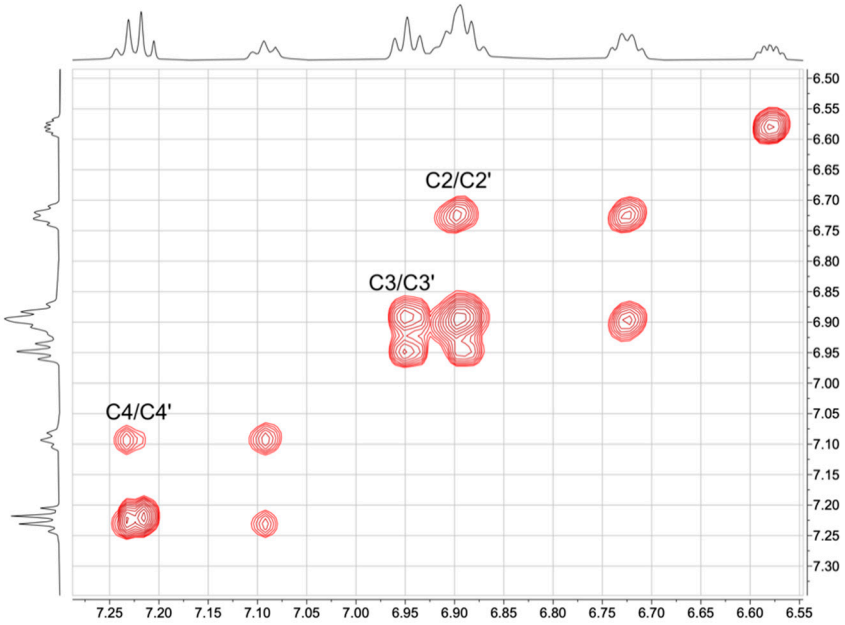

Figure 6. EXSY peaks in the NOESY spectrum (500 MHz, $C_2D_2Cl_4$, 328 K) of [Cu(xantphos)(biq)][PF_6] between resonances for pairs of phenyl protons.

3.3. Photophysical and Electrochemical Properties

The absorption spectra of [Cu(POP)(biq)][PF_6] and [Cu(xantphos)(biq)][PF_6] in CH_2Cl_2 solutions are shown in Figure 7 (red plots) and are compared with those of [Cu(POP)(bq)][PF_6] and [Cu(xantphos)(bq)][PF_6] (black curves). The absorption maxima are given in Table 2. Absorptions below 380 nm are assigned to ligand-based $\pi^*\leftarrow\pi$ transitions, while the broad bands in the visible region arise from MLCT from copper to π^* orbitals on the diimine ligand. The spectra for the 2,2'-biquinoline-containing compounds are in agreement with those previously published [15,17,18]. Figure 7 illustrates that incorporation of the bq ligand leads to a shift in the MLCT absorption to lower energies than that observed for [Cu(POP)(biq)][PF_6] and [Cu(xantphos)(biq)][PF_6]. This is rationalized in terms of the ring fusion in bq (Scheme 1) being adjacent to the N atoms but remote from the N atoms in biq (Scheme 2). An expansion of the MLCT regions is displayed in Figure S9. Excitation of deaerated CH_2Cl_2 solutions of [Cu(POP)(biq)][PF_6] and [Cu(xantphos)(biq)][PF_6] at wavelengths between 365 nm and 420 nm does not lead to an emission, and in the solid state, very weak emissions (PLQY < 1%) with λ_{max}^{em} = 650 nm for [Cu(POP)(biq)][PF_6] and 640 nm for [Cu(xantphos)(biq)][PF_6] were observed.

Significantly, the solid-state structure of [Cu(POP)(biq)][PF_6] reveals a short Cu···O distance (3.054(1) Å), as does the DFT energy minimized structure of [Cu(xantphos)(biq)]$^+$ (3.08 Å). An attempt to correlate solid-state PLQY values with Cu···O distances in [Cu(POP)(N^N)]$^+$ complexes concluded that there is a general trend for the highest PLQY values being associated with the longest Cu···O distances [37]. Thus, the short Cu···O distance in [Cu(POP)(biq)]$^+$ may contribute to the low PLQY value.

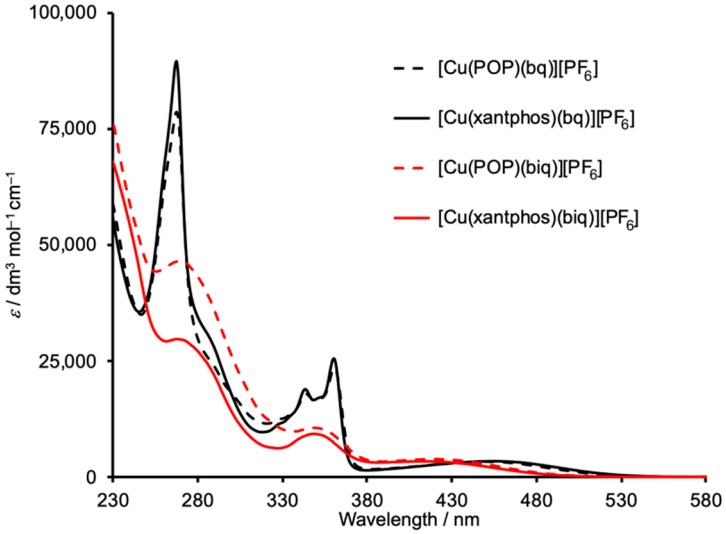

Figure 7. Solution absorption spectra of [Cu(POP)(biq)][PF_6] and [Cu(xantphos)(biq)][PF_6] compared to their 2,2'-biquinoline (bq) analogs (CH_2Cl_2, 2.5 × 10^{-5} mol dm^{-3}).

Table 2. Absorption maxima for CH_2Cl_2 solutions of [Cu(POP)(biq)][PF_6] and [Cu(xantphos)(biq)][PF_6] (2.5 × 10^{-5} mol dm^{-3}).

Compound	λ_{max}/nm (ε_{max}/dm³ mol⁻¹ cm⁻¹)	
	π*←π	MLCT
[Cu(POP)(biq)][PF_6]	273 (46,200), 352 (10,500)	423 (3800)
[Cu(xantphos)(biq)][PF_6]	272 (29,500), 353 (9100)	415 (3300)

The electrochemical behaviors of [Cu(POP)(biq)][PF_6] and [Cu(xantphos)(biq)][PF_6] were studied by cyclic voltammetry, and the results are presented in Table 3. Figure 8 illustrates the cyclic voltammogram (CV) of [Cu(POP)(biq)][PF_6]; that of the xantphos-containing compound is similar. Both compounds undergo a reversible oxidation process, which is ascribed to the Cu^+/Cu^{2+} couple. For both complexes, if the forward scan is extended above +1.2 V, another oxidation wave is observed at ca. +1.3 V. This process arises from the oxidation of the phosphane ligand. A reversible reduction process (Figure 8) is observed for each compound and is assigned to a biq-centered process. The copper (I) oxidations (Table 3) occur at lower potentials than in analogous complexes containing 2,2'-biquinoline (bq), consistent with the greater steric demands of the bq ligand compared to biq, which impede the flattening of the coordination sphere that accompanies copper (I) oxidation. Each of [Cu(POP)(bq)][PF_6] and [Cu(xantphos)(bq)][PF_6] is reported to undergo a quasi-reversible oxidation at +0.90 V and +0.95 V, respectively, in CH_2Cl_2 (Fc/Fc^+ reference) [17,18].

Table 3. Electrochemical processes in [Cu(POP)(biq)][PF_6] and [Cu(xantphos)(biq)][PF_6] (CH_2Cl_2 solutions, ca. 2×10^{-3} mol dm^{-3}); values referenced to internal $Fc/Fc^+ = 0.0$ V. [^{n}Bu$_4$N][PF_6] was the supporting electrolyte, and the scan rate was 0.1 V s^{-1}.

Compound	$E_{1/2}^{ox}$/V	E_{pc}–E_{pa}/mV	$E_{1/2}^{red}$/V	E_{pa}–E_{pc}/mV
[Cu(POP)(biq)][PF_6]	+0.74	111	–1.82	89
[Cu(xantphos)(biq)][PF_6]	+0.80	79	–1.74	98

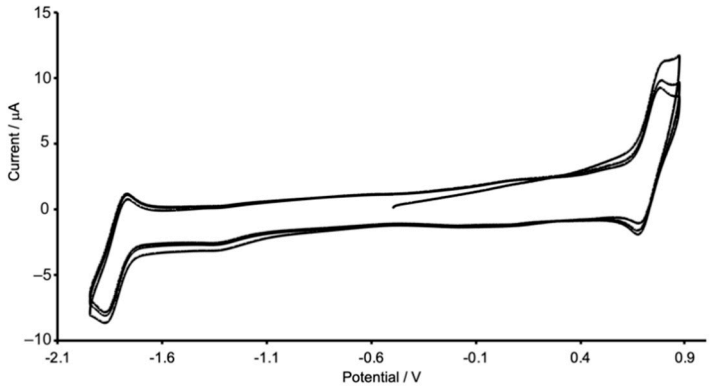

Figure 8. Three consecutive scans in the cyclic voltammogram of [Cu(POP)(biq)][PF_6] in CH_2Cl_2 solution; see Table 3 for additional details.

4. Conclusions

We report the preparation and characterization of [Cu(POP)(biq)][PF_6] and [Cu(xantphos)(biq)][PF_6], which are the first examples of [Cu(P^P)(N^N)]$^+$ complexes in which the N^N ligand is 1,1'-biisoquinoline. The single crystal structure of [Cu(POP)(biq)][PF_6] 0.5Et_2O was determined, confirming a distorted tetrahedral environment of the copper atom and non-coincidence of each Cu–N vector and the directionality of each sp^2 N lone pair. The Cu···O_{POP} distance is 3.054(1) Å, which is rather short when compared to other structurally characterized [Cu(P^P)(N^N)] cations. The structure of [Cu(POP)(biq)]$^+$ was compared to that of the analogous 2,2'-biquinoline (bq)-containing complex. The change in N^N ligand results in a smaller P–C–P angle in [Cu(POP)(biq)]$^+$ than in [Cu(POP)(bq)]$^+$, and there is a switch from an intra-ligand PPh_2-phenyl/$(C_6H_4)_2O$-arene π-stacking in [Cu(POP)(biq)]$^+$ to a π-stacking interaction between the POP and bq ligands in [Cu(POP)(bq)]$^+$, which is associated with the extended conjugation in the bq domain. Solution NMR spectroscopic data [Cu(POP)(biq)][PF_6] and [Cu(xantphos)(biq)][PF_6] are consistent with the compounds undergoing several dynamic processes. The photophysical and electrochemical behaviors of the heteroleptic copper (I) complexes were investigated, and the effects of changing from 2,2'-biquinoline to 1,1'-biisoquinoline were discussed. It is likely that the short Cu···O distances in [Cu(POP)(biq)]$^+$ and [Cu(xantphos)(biq)]$^+$ contribute to the very low PLQY values.

Supplementary Materials: The following are available online at www.mdpi.com/2073-4352/11/2/185/s1, Figures S1–S2: Mass spectra; Figure S3: Additional structural diagram of the [Cu(POP)(biq)]$^+$ cation; Figures S4–S8: NMR spectra; Figure S9: Expansion of the MLCT region in solution absorption spectra; Table S1: Cartesian coordinates for the modelled structure of [Cu(xantphos)(biq)]$^+$.

Author contributions: project conceptualization, administration, supervision, and funding acquisition, E.C.C. and C.E.H.; investigation and data analysis, N.A. and M.M.; crystallography, A.P.; structure analysis and writing, C.E.H.; manuscript editing, N.A., M.M., A.P., and E.C.C. All authors have read and agreed to the published version of the manuscript.

Funding: This research was funded in part by the Swiss National Science Foundation, grant number 200020_182000.

Acknowledgments: We thank the University of Basel for support of our research.

Data Availability Statement: The data presented in this study are available on request from the corresponding author. The data are not publicly accessible at present.

Conflicts of Interest: The authors declare no conflict of interest.

References

1. Buckner, M.T.; McMillin, D.R. Photoluminescence from copper(I) complexes with low-lying metal-to-ligand charge transfer excited states. *J. Chem. Soc. Chem. Commun.* **1978**, 759–761, doi:10.1039/c39780000759.
2. Rader, R.A.; McMillin, D.R.; Buckner, M.T.; Matthews, T.G.; Casadonte, D.J.; Lengel, R.K.; Whittaker, S.B.; Darmon, L.M.; Lytle, F.E. Photostudies of 2,2′-bipyridine bis(triphenylphosphine)copper(1+), 1,10-phenanthroline bis(triphenylphosphine)copper(1+), and 2,9-dimethyl-1,10-phenanthroline bis(triphenylphosphine)copper(1+) in solution and in rigid, low-temperature glasses. Simultaneous multiple emissions from intraligand and charge-transfer states. *J. Am. Chem. Soc.* **1981**, *103*, 5906–5912, doi:10.1021/ja00409a048.
3. Armaroli, N.; Accorsi, G.; Cardinali, F.; Listorti, A. Photochemistry and Photophysics of Coordination Compounds: Copper. *Top. Curr. Chem.* **2007**, *280*, 69–115, doi:10.1007/128_2007_128.
4. Costa, R.D.; Ortí, E.; Bolink, H.J.; Monti, F.; Accorsi, G.; Armaroli, N. Luminescent Ionic Transition-Metal Complexes for Light-Emitting Electrochemical Cells. *Angew. Chem. Int. Ed.* **2012**, *51*, 8178–8211, doi:10.1002/anie.201201471.
5. Costa, R.D. (Ed.) *Light-Emitting Electrochemical Cells: Concepts, Advances and Challenges*; Springer International Publishing: New York, NY, USA, 2017, doi: 10.1007/978-3-319-58613-7.
6. Fresta, E.; Costa, R.D. Beyond traditional light-emitting electrochemical cells—A review of new device designs and emitters. *J. Mater. Chem. C* **2017**, *5*, 5643–5675, doi:10.1039/c7tc00202e.
7. Costa, R.D.; Tordera, D.; Ortí, E.; Bolink, H.J.; Schönle, J.; Graber, S.; Housecroft, C.E.; Constable, E.C.; Zampese, J.A. Copper(i) complexes for sustainable light-emitting electrochemical cells. *J. Mater. Chem.* **2011**, *21*, 16108–16118, doi:10.1039/c1jm12607e.
8. Czerwieniec, R.; Leitl, M.J.; Homeier, H.H.; Yersin, H. Cu(I) complexes—Thermally activated delayed fluorescence. Photophysical approach and material design. *Co-ord. Chem. Rev.* **2016**, *325*, 2–28, doi:10.1016/j.ccr.2016.06.016.
9. Minozzi, C.; Caron, A.; Grenier-Petel, J.-C.; Santandrea, J.; Collins, S.K. Heteroleptic Copper(I)-Based Complexes for Photocatalysis: Combinatorial Assembly, Discovery, and Optimization. *Angew. Chem. Int. Ed.* **2018**, *57*, 5477–5481, doi:10.1002/anie.201800144.
10. Hernandez-Perez, A.C.; Collins, S.K. Heteroleptic Cu-Based Sensitizers in Photoredox Catalysis. *Acc. Chem. Res.* **2016**, *49*, 1557–1565, doi:10.1021/acs.accounts.6b00250.
11. Zhang, Y.; Schulz, M.; Wächtler, M.; Karnahl, M.; Dietzek, B. Heteroleptic diimine–diphosphine Cu(I) complexes as an alternative towards noble-metal based photosensitizers: Design strategies, photophysical properties and perspective applications. *Co-ord. Chem. Rev.* **2018**, *356*, 127–146, doi:10.1016/j.ccr.2017.10.016.
12. Keller, S.; Constable, E.C.; Housecroft, C.E.; Neuburger, M.; Prescimone, A.; Longo, G.; Pertegás, A.; Sessolo, M.; Bolink, H.J. [Cu(bpy)(P^P)]+ containing light-emitting electrochemical cells: Improving performance through simple substitution. *Dalton Trans.* **2014**, *43*, 16593–16596, doi:10.1039/c4dt02847c.
13. Alkan-Zambada, M.; Keller, S.; Martinez-Sarti, L.; Prescimone, A.; Junquera-Hernandez, J.M.; Constable, E.C.; Bolink, H.J.; Sessolo, M.; Orti, E.; Housecroft, C.E. [Cu(P^P)(N^N)][PF6] compounds with bis(phosphane) and 6-alkoxy, 6-alkylthio, 6-phenyloxy and 6-phenylthio-substituted 2,2′-bipyridine ligands for light-emitting electrochemical cells. *J. Mater. Chem. C* **2018**, *6*, 8460–8471, doi:10.1039/c8tc02882f.
14. Keller, S.; Pertegás, A.; Longo, G.; Martínez, L.; Cerdá, J.; Junquera-Hernández, J.M.; Prescimone, A.; Constable, E.C.; Housecroft, C.E.; Ortí, E.; et al. Shine bright or live long: Substituent effects in [Cu(N^N)(P^P)]+-based light-emitting electrochemical cells where N^N is a 6-substituted 2,2′-bipyridine. *J. Mater. Chem. C* **2016**, *4*, 3857–3871, doi:10.1039/c5tc03725e.
15. Zhang, Q.; Ding, J.; Cheng, Y.; Wang, L.; Xie, Z.; Jing, X.; Wang, F. Novel Heteroleptic CuI Complexes with Tunable Emission Color for Efficient Phosphorescent Light-Emitting Diodes. *Adv. Funct. Mater.* **2007**, *17*, 2983–2990, doi:10.1002/adfm.200601053.
16. Luo, S.-P.; Chen, N.-Y.; Sun, Y.-Y.; Xia, L.-M.; Wu, Z.-C.; Junge, H.; Beller, M.; Wu, Q.-A. Heteroleptic copper(I) photosensitizers of dibenzo[b,j]-1,10-phenanthroline derivatives driven hydrogen generation from water reduction. *Dye. Pigment.* **2016**, *134*, 580–585, doi:10.1016/j.dyepig.2016.07.040.
17. McCullough, B.J.; Neyhouse, B.J.; Schrage, B.R.; Reed, D.T.; Osinski, A.J.; Ziegler, C.J.; White, T.A. Visible-Light-Driven Photosystems Using Heteroleptic Cu(I) Photosensitizers and Rh(III) Catalysts To Produce H2. *Inorg. Chem.* **2018**, *57*, 2865–2875, doi:10.1021/acs.inorgchem.7b03273.
18. Saeedi, S.; Xue, C.; McCullough, B.J.; Roe, S.E.; Neyhouse, B.J.; White, T.A. Probing the Diphosphine Ligand's Impact within Heteroleptic, Visible-Light-Absorbing Cu(I) Photosensitizers for Solar Fuels Production. *ACS Appl. Energy Mater.* **2018**, *2*, 131–143, doi:10.1021/acsaem.8b02098.

19. Kubiček, K.; Veedu, S.T.; Storozhuk, D.; Kia, R.; Techert, S. Geometric and electronic properties in a series of phosphorescent heteroleptic Cu(I) complexes: Crystallographic and computational studies. *Polyhedron* **2017**, *124*, 166–176, doi:10.1016/j.poly.2016.12.035.
20. Fresta, E.; Weber, M.D.; Fernandez-Cestau, J.; Costa, R.D. White Light-Emitting Electrochemical Cells Based on Deep-Red Cu(I) Complexes. *Adv. Opt. Mater.* **2019**, *7*, 1900830, doi:10.1002/adom.201900830.
21. Saeedi, S.; White, T.A. Cu(I) photosensitizers with alkylated diphosphines: Towards enhancing photostability and architecture extension. *Inorga. Chim. Acta* **2020**, *512*, 119876, doi:10.1016/j.ica.2020.119876.
22. Cuttell, D.G.; Kuang, S.-M.; Fanwick, P.E.; McMillin, D.R.; Walton, R.A. Simple Cu(I) Complexes with Unprecedented Excited-State Lifetimes. *J. Am. Chem. Soc.* **2002**, *124*, 6–7, doi:10.1021/ja012247h.
23. Kuang, S.-M.; Cuttell, D.G.; McMillin, D.R.; Fanwick, P.E.; Walton, R.A. Synthesis and Structural Characterization of Cu(I) and Ni(II) Complexes that Contain the Bis[2-(diphenylphosphino)phenyl]ether Ligand. Novel Emission Properties for the Cu(I) Species. *Inorg. Chem.* **2002**, *41*, 3313–3322, doi:10.1021/ic0201809.
24. Eliel, E.L.; Wilen, S.H. *Stereochemistry of Organic Compounds*; John Wiley & Sons: New York, NY, USA, 1994; p 1267., ISBN: 978-0-471-01670-0.
25. Crawford, M.; Smyth, I.F.B. The optical resolution and racemisation of some diisoquinolyls. *J. Chem. Soc.* **1954**, 3464–3468, doi:10.1039/jr9540003464.
26. Jahng, Y.; Park, J.G.; Yu, J.W. Synthesis and Properties of Cu(I) Complexes of Isoquinoline-Related Bidentates. *Bull. Korean Chem. Soc.* **2000**, *21*, 333–335.
27. Attenberger, B.; Moussa, M.E.S.; Brietzke, T.; Vreshch, V.; Holdt, H.-J.; Lescop, C.; Scheer, M. Discrete Polymetallic Arrangements of Ag I and Cu I Ions Based on Multiple Bridging Phosphane Ligands and π-π Interactions. *Eur. J. Inorg. Chem.* **2015**, *2015*, 2934–2938, doi:10.1002/ejic.201500445.
28. Kammer, S.; Kelling, A.; Baier, H.; Mickler, W.; Dosche, C.; Rurack, K.; Kapp, A.; Lisdat, F.; Holdt, H.-J. 2,11-Dialkylated 1,12-Diazaperylene Copper(I) Complexes: First Supramolecular Column Assemblies by π-π Stacking between Homoleptic Tetrahedral Metal Complexes, Exhibiting Low-Energy MLCT Transitions. *Eur. J. Inorg. Chem.* **2009**, *2009*, 4648–4659, doi:10.1002/ejic.200900695.
29. Kubas, G.J.; Monzyk, B.; Crumbliss, A.L. Tetrakis(Acetonitrile)Copper(I) Hexafluorophosphate. *Inorg. Synth.* **2007**, *19*, 90–92, doi:10.1002/9780470132500.ch18.
30. Palatinus, L.; Chapuis, G. SUPERFLIP– a computer program for the solution of crystal structures by charge flipping in arbitrary dimensions. *J. Appl. Crystallogr.* **2007**, *40*, 786–790, doi:10.1107/s0021889807029238.
31. Palatinus, L.; Prathapa, S.J.; Van Smaalen, S. EDMA: A computer program for topological analysis of discrete electron densities. *J. Appl. Crystallogr.* **2012**, *45*, 575–580, doi:10.1107/s0021889812016068.
32. Dolomanov, O.V.; Bourhis, L.J.; Gildea, R.J.; Howard, J.A.K.; Puschmann, H. OLEX2: A complete structure solution, refinement and analysis program. *J. Appl. Crystallogr.* **2009**, *42*, 339–341, doi:10.1107/s0021889808042726.
33. Macrae, C.F.; Edgington, P.R.; McCabe, P.; Pidcock, E.; Shields, G.P.; Taylor, R.D.; Towler, M.; Van De Streek, J. Mercury: Visualization and analysis of crystal structures. *J. Appl. Crystallogr.* **2006**, *39*, 453–457, doi:10.1107/s002188980600731x.
34. Macrae, C.F.; Sovago, I.; Cottrell, S.J.; Galek, P.T.A.; McCabe, P.; Pidcock, E.; Platings, M.; Shields, G.P.; Stevens, J.S.; Towler, M.; et al. Mercury 4.0: From visualization to analysis, design and prediction. *J. Appl. Crystallogr.* **2020**, *53*, 226–235, doi:10.1107/s1600576719014092.
35. Nishio, M. CH/? hydrogen bonds in crystals. *CrystEngComm* **2004**, *6*, 130–158, doi:10.1039/b313104a.
36. Nishio, M.; Umezawa, Y.; Honda, K.; Tsuboyama, S.; Suezawa, H. CH/π hydrogen bonds in organic and organometallic chemistry. *CrystEngComm* **2009**, *11*, 1757–1788, doi:10.1039/b902318f.
37. Keller, S.; Alkan-Zambada, M.; Prescimone, A.; Constable, E.C.; Housecroft, C.E. Extended π-Systems in Diimine Ligands in [Cu(P^P)(N^N)][PF6] Complexes: From 2,2′-Bipyridine to 2-(Pyridin-2-yl)Quinoline. *Crystals* **2020**, *10*, 255, doi:10.3390/cryst10040255.
38. Ashby, M.T.; Govindan, G.N.; Grafton, A.K. Metal-Assisted Racemization of the Atropisomers of a 1,1′-Binaphthyl Skeleton via a Syn Transition State. *J. Am. Chem. Soc.* **1994**, *116*, 4801–4809, doi:10.1021/ja00090a028.
39. Groom, C.R.; Bruno, I.J.; Lightfoot, M.P.; Ward, S.C. The Cambridge Structural Database. *Acta Crystallogr. Sect. B Struct. Sci. Cryst. Eng. Mater.* **2016**, *72*, 171–179, doi:10.1107/s2052520616003954.
40. Bruno, I.J.; Cole, J.C.; Edgington, P.R.; Kessler, M.; Macrae, C.F.; McCabe, P.; Pearson, J.; Taylor, R. New software for searching the Cambridge Structural Database and visualizing crystal structures. *Acta Crystallogr. Sect. B Struct. Sci.* **2002**, *58*, 389–397, doi:10.1107/s0108768102003324.
41. Sun, L.-Z.; Wang, S.L.; Liu, J.-M.; Li, Z.-F.; Zhang, J.-W.; Jin, Q.-H. Synthesis, Characterization and Luminescent Properties of Two Copper(I) Complexes Based on 2,2′-Biquinoline and Phosphorus Ligand. *Jiegou Huaxue* **2018**, *37*, 1313, doi:10.14102/j.cnki.0254-5861.2011-1942.
42. Spartan'18 v. 1.4.4; Wavefunction, Inc.: Irvine, CA, USA. Available online: https://www.wavefun.com/spartan-latest-version (access on 27 January 2021).

43. Meyer, M.; Brunner, F.; Prescimone, A.; Constable, E.C.; Housecroft, C.E. Desymmetrizing Heteroleptic [Cu(P^P)(N^N)][PF_6] Compounds: Effects on Structural and Photophysical Properties, and Solution Dynamic Behavior. *Molecules* **2020**, *26*, 125, doi:10.3390/molecules26010125.
44. Bardají, M.; Miguel-Coello, A.B.; Espinet, P. Mono- and dinuclear luminescent 1,1'-biisoquinoline gold(I) complexes. *Inorg. Chim. Acta* **2012**, *392*, 91–98, doi:10.1016/j.ica.2012.06.024.